Design and Fabrication of 3D Fingerprint Targets

Sunpreet S. Arora, *Student Member, IEEE,* Kai Cao, Anil K. Jain, *Life Fellow, IEEE,*
and Nicholas G. Paulter Jr., *Fellow, IEEE*

Abstract—Standard targets are typically used for structural (white-box) evaluation of fingerprint readers, e.g., for calibrating imaging components of a reader. However, there is no standard method for behavioral (black-box) evaluation of fingerprint readers in operational settings where variations in finger placement by the user are encountered. The goal of this research is to design and fabricate 3D targets for repeatable behavioral evaluation of fingerprint readers. 2D calibration patterns with known characteristics (e.g. sinusoidal gratings of pre-specified orientation and frequency, fingerprints with known singular points and minutiae) are projected onto a generic 3D finger surface to create electronic 3D targets. A state-of-the-art 3D printer (Stratasys Objet350 Connex) is used to fabricate wearable 3D targets with materials similar in hardness and elasticity to the human finger skin. The 3D printed targets are cleaned using 2M NaOH solution to obtain evaluation-ready 3D targets. Our experimental results show that (i) features present in the 2D calibration pattern are preserved during the creation of the electronic 3D target, (ii) features engraved on the electronic 3D target are preserved during the physical 3D target fabrication, and (iii) intra-class variability between multiple impressions of the physical 3D target is small. We also demonstrate that the generated 3D targets are suitable for behavioral evaluation of three different (500/1000 ppi) PIV/Appendix F certified optical fingerprint readers in the operational settings.

Keywords—*3D fingerprint targets, fingerprint reader evaluation, 2D calibration patterns, 3D printing, 2D pattern to 3D surface projection.*

I. INTRODUCTION

STRUCTURAL (white-box) evaluation[1] of imaging systems is generally done using specially designed objects with known properties, called *targets*. In the biomedical domain, for instance, such objects (called *phantoms*) are used for calibrating and testing optical measurement profiles of sensing instrumentation [3], [4]. Similarly, targets (Fig. 1) have also been used for calibration of fingerprint readers.

There are two separate standards currently in use by the Federal Bureau of Investigation (FBI) for the certification of fingerprint readers, (i) the *PIV*, which caters to single-finger readers designed for applications involving person verification (one-to-one comparison), and (ii) the *Appendix F,*

S. S. Arora, K. Cao and A. K. Jain are with the Department of Computer Science and Engineering, Michigan State University, East Lansing, MI, 48824. E-mail: {arorasun, kaicao, jain}@cse.msu.edu

N. G. Paulter Jr. is with the National Institute of Standards and Technology, 100 Bureau Dr., Gaithersburg, MD, 20899. E-mail: paulter@nist.gov

[1]Structural or white-box evaluation tests how internal system components and component sub-assemblies should operate, and requires technical knowledge of the system [2].
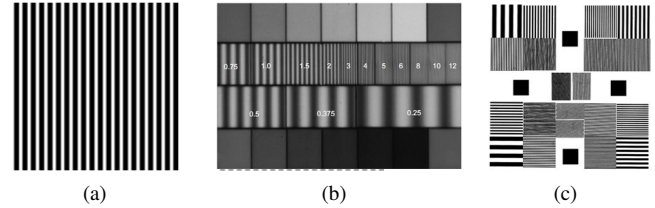

Fig. 1: 2D images of standard targets used for calibrating fingerprint readers, (a) ronchi (vertical bar) target for calibrating the geometric accuracy, (b) sine wave target for measuring the resolution, and (c) multiple bar target for estimating the spatial frequency response of a fingerprint reader (images taken from [6]).

which applies to fingerprint readers designed for use in large scale applications involving person identification (one-to-many comparisons) [5]. To get their fingerprint readers certified, fingerprint vendors need to demonstrate that the images captured using their readers meet the image quality specifications laid out in the relevant standard [6] [7]. A typical procedure is (i) to use 2D/3D calibration targets to ascertain if the images of the targets captured using the reader meet the specifications, (ii) modify the reader configuration, if needed, to ensure it captures images of sufficient quality to meet the specifications, and (iii) when satisfied with the reader configuration, submit test images to the testing agency for review[2] [5]. If the test data is found to meet the desired specifications, the testing agency certifies the fingerprint reader as being compliant with the specific standard.

Standard calibration targets (see Fig. 1) are used for structural evaluation of fingerprint readers. For example, the targets in [9] are utilized for testing frustrated total internal reflection (FTIR) components (LED, glass prism and platen assembly) of an optical fingerprint reader. However, these targets are not suitable for behavioral (black-box) evaluation[3] of a fingerprint reader in the presence of operational variations (e.g., finger placement and pressure etc.) when users interact with the reader. This is because these targets are not specifically constructed using materials with properties (e.g., hardness and elasticity) similar to the human finger skin.

For behavioral evaluation of a fingerprint reader, one possibility is to conduct pilot studies in the field using the reader. This, however, is a tedious process both in terms of time and resource commitment, and is limited by the amount and

[2]Review of the submitted test data is conducted by the Technology Evaluation Standards Test Unit, a part of the FBI's Biometric Center of Excellence (BCOE) led by the Criminal Justice Information (CJI) Services Division [8].

[3]Behavioral or black-box evaluation tests functions supported by the system in the operational or deployment scenario by focusing on the input and output of the system [2].
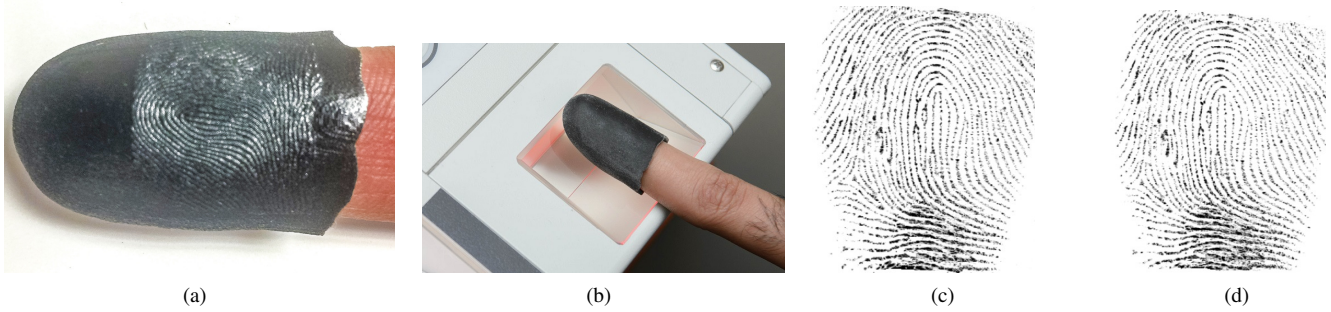
Fig. 2: Evaluating an optical fingerprint reader using the 3D targets designed and fabricated by the authors. (a) The 3D target is worn on a finger, (b) the finger is placed on the fingerprint reader platen, and (c)-(f) multiple 2D impressions (two shown here) of the 3D target are captured to evaluate the reader.

possible variations in the fingerprint data that can be collected. Besides, such a procedure cannot be used for repeatable behavioral evaluation of the fingerprint reader because, in practice, the same set of subjects is typically not available for repeat testing. The goal of this research, therefore, is to fabricate standard 3D targets which can be used for repeatable behavioral evaluation of fingerprint readers. We fabricate 3D targets with material similar in hardness and elasticity to the human finger skin such that they can be worn on a finger and placed on the fingerprint reader platen in a natural manner (see Fig. 2). Because the purpose of generating 3D targets is to assess the image capture fidelity of different fingerprint readers, it is necessary to develop a set of patterns, not all of which must be fingerprints, to adequately represent the types of features that are presented to fingerprint readers. 3D targets generated using such patterns can be used to comprehensively evaluate the imaging capability of fingerprint readers. Accordingly, the 3D targets do not need to incorporate other finger parts, such as fingertips or the palm-side surfaces from the distal to the proximal interphalangeal joints.

The utility of the fabricated 3D targets extends beyond behavioral evaluation of fingerprint readers. 3D targets generated using 2D synthetic fingerprint images with known fingerprint features (e.g. fingerprint type (loop, whorl, arch), minutiae position and orientation, and core and delta count and locations) can be used to evaluate fingerprint feature extraction and matching algorithms. Such targets can, therefore, be used for end-to-end evaluation of a fingerprint recognition system from placing the finger on the reader and capturing the 2D impression to extracting features and comparing the captured image to the gallery templates. Further, since the fabricated 3D targets are similar in characteristics to the human finger skin, in our opinion, they can also be used to evaluate the next generation touchless fingerprint readers [13] [14] [15]. Hence the proposed 3D targets are better suited for fingerprint system evaluation purposes than the prevailing methods which only use 2D synthesized fingerprint images (see Table I).

A physical 3D target is created by first projecting an electronic 2D calibration pattern onto a generic electronic 3D

model of the finger surface[4]. The electronic 3D finger surface is aligned such that the finger length is along the y-axis, width along the x-axis and depth along the z-axis. The electronic 3D surface is then preprocessed to ensure sufficient fidelity for establishing the correspondence between the electronic 2D calibration pattern and the electronic 3D finger surface. The 2D calibration pattern is then mapped onto the front portion of the electronic 3D surface and correspondences between each vertex on the frontal electronic 3D surface and the pixel locations in the 2D calibration pattern are established. The 2D calibration pattern is engraved onto the frontal electronic 3D finger surface by displacing each vertex along the surface normal according to the texture values at the mapped pixel locations. Finally, the electronic 3D finger surface is post-processed to create an electronic model of a wearable 3D target ready for 3D printing. The physical 3D targets are fabricated using a state-of-the-art 3D printer (Stratasys Objet350 Connex[5]) with material similar in hardness and elasticity to the human finger skin. The 3D printed targets are cleaned using a 2M NaOH solution to generate evaluation-ready physical 3D targets. The complete process is illustrated in Fig. 3.

We perform experiments to assess the fidelity of the 3D target generation process by (i) estimating the 2D to 3D projection error of the mapping algorithm used in electronic 3D target creation, (ii) estimating the 3D printing fabrication error by observing the targets under a digital optical microscope (Keyence Digital Microscope VHX 600 [17]), (iii) matching 2D calibration pattern features used for 3D target creation to both the electronic and physical 3D target images, and (iv) evaluating similarity between different images of physical 3D targets. We show that (i) features present in the 2D calibration pattern are preserved during the creation of electronic 3D target, (ii) features engraved on the electronic 3D target are preserved during physical 3D target fabrication, and (iii) intra-class variability between multiple impressions of the same

---

[4]The 3D finger surface could either be the shape of the finger sensed using a 3D scanner or a synthetically generated surface describing the shape of the finger. In our case, the finger surface was scanned using the Artec Eva 3D scanner [16].

[5]The naming of companies and products here does not imply endorsement or recommendation of those companies or products by the authors or the organizations they represent.

TABLE I: Comparison of prevailing 2D synthetic fingerprint based evaluation methods with the proposed 3D target generation method.

Method	Artifacts*	Fingerprint Features	Evaluation Use Cases
SFinGe [10]	2D synthetic fingerprints (electronic)	Known fingerprint ridge flow and ridge density features; uncontrolled minutiae placement	Fingerprint feature extractors and matchers
IBG DHS SBIR [11]	2D synthetic fingerprints (electronic)	Known fingerprint ridge flow and ridge density features; partially controlled minutiae placement	Fingerprint feature extractors and matchers
Zhao et al. [12]	2D synthetic fingerprints (electronic)	Known fingerprint ridge flow, ridge density and minutiae placement	Fingerprint feature extractors and matchers
Proposed	3D targets (electronic and physical)	Known fingerprint ridge flow, ridge density and minutiae placement	End-to-end fingerprint systems, including fingerprint readers, feature extractors and matchers

*The term *electronic* is used for digitally generated artifacts, whereas the term *physical* is used for physically fabricated artifacts from electronic artifacts.
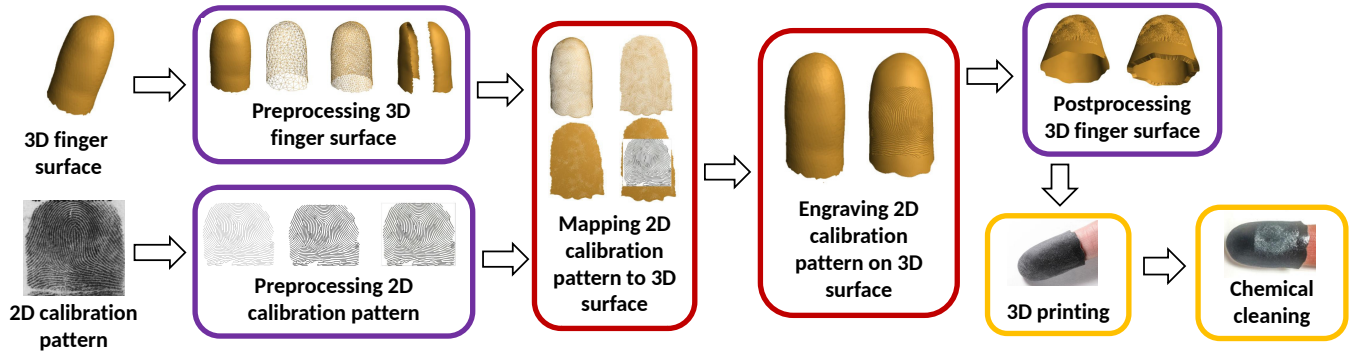
Fig. 3: Generating a 3D fingerprint target A, given a 2D calibration pattern I and a 3D finger surface S.

physical 3D target is sufficiently small for matching at false accept rate (FAR) of 0.01%. We also show that the generated 3D targets are suitable for behavioral evaluation of three different (500/1000 ppi) PIV/Appendix F certified optical fingerprint readers in the operational settings.

In summary, the contributions of this research are as follows:

- Design of wearable 3D targets using a 2D to 3D projection algorithm that preserves distances on the 2D calibration pattern while mapping it to 3D finger surface. The projection algorithm used in our preliminary work [1] did not preserve the distances near the periphery of the 3D surface.
- Fabrication of 3D targets using a state-of-the-art 3D printer with materials having similar hardness and elasticity to the human finger skin. These targets can be imaged by three different commercial (500/1000 ppi) optical fingerprint readers. The 3D printer used to fabricate targets in [1] only printed hard plastic targets that could not be imaged by commercial fingerprint readers.
- Procedure to chemically clean the 3D printed targets without impacting the engraved target patterns.
- Estimation of (i) 2D to 3D projection and (ii) 3D printing fabrication errors; these errors are accounted for during fingerprint reader evaluations.
- Comprehensive experimentation to show the fidelity of 2D calibration pattern features during 3D target generation.

- Behavioral evaluation of fingerprint readers using the generated 3D targets.

II. GENERATING 3D TARGETS

A 3D target A is generated using a 2D calibration pattern I with pre-specified features, and a generic 3D finger surface S. Let the grayscale value in the 2D calibration pattern I at spatial coordinates (u, v) be denoted by $I(u, v)$. Also, assume that the 3D finger surface S is a triangular mesh with a set V of vertices and a set T of triangles. Each vertex, v, in V has (x, y, z) coordinates corresponding to its spatial location in S, and a triangle in T connects a unique set of three vertices. Generating the 3D target A using I and S then consists of the following main steps (Fig. 3).

A. Preprocessing 3D finger surface

A sequence of preprocessing steps is executed on the 3D finger surface S before projecting the 2D calibration pattern I on S (see Fig. 4).

Alignment: The 3D finger surface S, arbitrarily oriented in the (x, y, z) coordinate frame, is first aligned such that the finger length is along the y-axis, width along the x-axis and height on the z-axis. For doing this, each vertex in the set V is translated such that the center of the surface S coincides with the origin of the (x, y, z) coordinate axes. Principal component analysis (PCA) [18] is used to determine the principle directions of the surface spread. The computed
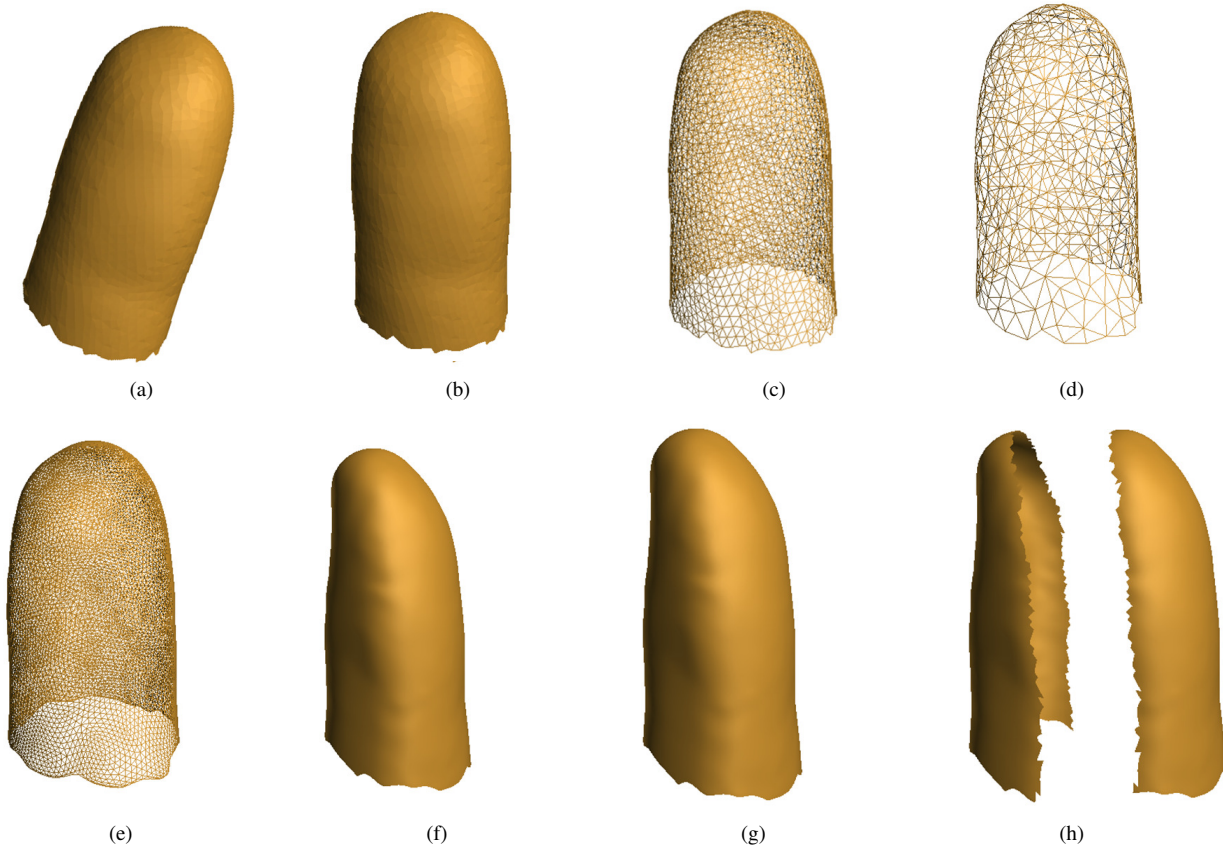
Fig. 4: Preprocessing 3D finger surface. (a) Original finger surface S, (b) aligning S such that the finger length is along the y axis, (c) aligned S (triangular mesh), (d) remeshing S (triangular mesh), (e) subdividing S (triangular mesh), (f) subdivided S (profile view), (g) creating outer finger surface S_O from (f), and (h) separating front and rear portions, S_{OF} and S_{OR}, of S_O.

principal components are then used to align the surface S. Note that this step only alters the absolute (x, y, z) coordinate values of the vertices in V and retains the geometry of the surface S.

Remeshing: The 3D finger surface S is remeshed by sampling vertices from V using the method in [19]. The first vertex v_1 is sampled randomly from V, and the geodesic distance map $U(v_1)$ from v_1 to every other vertex in V is computed by solving the eikonal equation using the fast marching method [20]:

$$|| \bigtriangledown U(v_1)|| = P(v_1). \qquad (1)$$

Here, $\bigtriangledown$ is the gradient operator, and $P = 1/F$, where F is the speed of front propagation used in the fast marching method.

Vertices are then sampled iteratively by adding the farthest vertex among the remaining vertices in iteration i from the vertices in the sampled vertex set V_{i-1} at iteration $i-1$. Note that the geodesic distance map U_i, at iteration i, is updated using the following equation:

$$U_i = min(U_{i-1}, U(v_i)), \qquad (2)$$

where $U(v_i)$ is the geodesic distance map of the vertex sampled at iteration i, and U_{i-1} is the geodesic distance map computed at iteration $i-1$.

During this iterative procedure of sampling vertices, the speed of front propagation F is set to $1/(1 + C)$, where C is the aggregate curvature at each vertex in V. This results in more vertices being sampled in the higher curvature regions of the 3D surface and vice versa. The aggregate curvature C is calculated using the two principal curvatures C_{min} and C_{max} as follows,

$$C = |C_{min}| + |C_{max}|. \qquad (3)$$

Here, $| . |$ is the absolute value operator, C_{min} and C_{max} are computed from the 3D curvature tensor C_T calculated using the method in [21]. In particular, C_{min} and C_{max} correspond to the two highest eigenvalues of the curvature tensor C_T.

Finally, Delaunay triangulation is used for recreating the remeshed surface from the set of sampled vertices [22].

Subdivision: Although remeshing makes the surface S uniformly dense depending on its curvature, it reduces the density of the vertices. To ensure sufficient fidelity for projecting the

Fig. 5: Preprocessing a 2D fingerprint pattern before projecting it onto 3D finger surface. (a) Original fingerprint image I, (b) extracted skeleton I_S of the fingerprint in (a), (c) skeleton I_S in (b) after applying the morphological operation of dilation, and (d) dilated skeleton in (c) smoothed using a gaussian filter.

2D calibration pattern I onto the surface S, Loop's surface subdivision method [23] is used to increase density of vertices. Let the set of vertices and triangles obtained after remeshing be denoted by V_R and T_R, respectively. This method creates new vertices at each edge of every triangle in T_R using a weighted combination of neighborhood vertices, and creates new triangles by connecting the sampled vertices at edges adjacent to each other. The original vertices are then translated to maintain surface smoothness and continuity.

Creating outer surface: Let V_S and T_S be the set of vertices and triangles obtained after surface subdivision. Let the normal n at a vertex v in the set V_S be denoted by (n_x, n_y, n_z), where n_x, n_y and n_z represent the normal components along the x, y and z directions, respectively. Each vertex v is then displaced by a fixed factor d along the normal n to obtain the displaced coordinates of the vertex (v'_x, v'_y, v'_z):

$$\begin{bmatrix} v'_x \\ v'_y \\ v'_z \end{bmatrix} = \begin{bmatrix} v_x \\ v_y \\ v_z \end{bmatrix} + \begin{bmatrix} n_x \\ n_y \\ n_z \end{bmatrix} \times d \qquad (4)$$

This is done to create an outer finger surface S_O where the 2D calibration pattern will be projected. The parameter d determines the thickness of the 3D target. Ideally, it is desirable to set d to be as small as possible. However, due to the limitation of the 3D printer resolution used for fabricating the targets, choosing a very small d results in the printed model being fragile. Therefore, d is empirically set to 1.5 mm in our experiments.

Separating front and rear portions: Front and rear portions of the outer finger surface S_O are then separated by computing the surface normals at each triangle in T_S, and then retaining the triangles and corresponding vertices where surface normals have the z-component greater than 0 in the front surface, and the rest in the rear surface. Note that the alignment of the finger surface done in step 1) facilitates this separation process. Let us denote the front portion of the outer surface S_O as S_{OF} having the set of vertices V_{OF} and triangles T_{OF}. Similarly, let the rear portion be denoted as S_{OR} with the set of vertices V_{OR} and triangles T_{OR}. We also retain the original finger surface S with the set of vertices V_S and triangles T_S.

B. Preprocessing 2D calibration pattern

If the pattern I being projected on 3D frontal surface S_{OF} is a fingerprint image, the following preprocessing steps are executed on I (see Fig. 5):

1) The skeleton, I_S, of I, a 1-pixel wide ridge pattern, is extracted using a commercial fingerprint SDK [24].
2) The ridge width on the skeleton I_S is increased to 3 pixels by performing the morphological operation of dilation using a 2 pixel radius disk structured element.
3) I_S is filtered using a 4×4 Gaussian filter with $\sigma = 2.5$ to ensure that ridges and valleys in 2D fingerprint pattern I are engraved smoothly onto the 3D finger surface.

This preprocessing is not needed for other calibration patterns (e.g. sine grating of certain orientation and spacing).

C. Mapping 2D calibration pattern to 3D surface

The front portion S_{OF} of the outer finger surface S_O is projected from 3D ((x, y, z) space) to 2D ((u, v) space) by computing the ISOMAP embedding [25] (see Fig. 6). Recall that the vertices and triangles in S_{OF} are V_{OF} and T_{OF}, respectively. The ISOMAP embedding is computed by:

1) **Constructing adjacency graph**: An adjacency graph G is created by connecting all vertex pairs $\{v_i, v_j\}$ in V_{OF} that share an edge of any triangle in T_{OF}. The edge weights in G are set to the euclidean distance $D(v_i, v_j)$ between v_i and v_j. For non-adjacent vertex pairs that do not share any edge, D is set to an arbitrary large value.
2) **Computing shortest paths**: Dijkstra's shortest path algorithm [26] is used to compute the shortest path between all pairs of nodes in G. Geodesic distances between all pairs of vertices in V_{OF} are estimated by the shortest path distances of the nodes in G.
3) **Constructing 2D embedding**: Let the matrix D_G contain the shortest path distances computed in the previous step. Given D_G, multidimensional scaling (MDS) [27] is used to create the 2D embedding of vertices. ISOMAP embedding is used because it minimizes the distortion induced when projecting the front portion
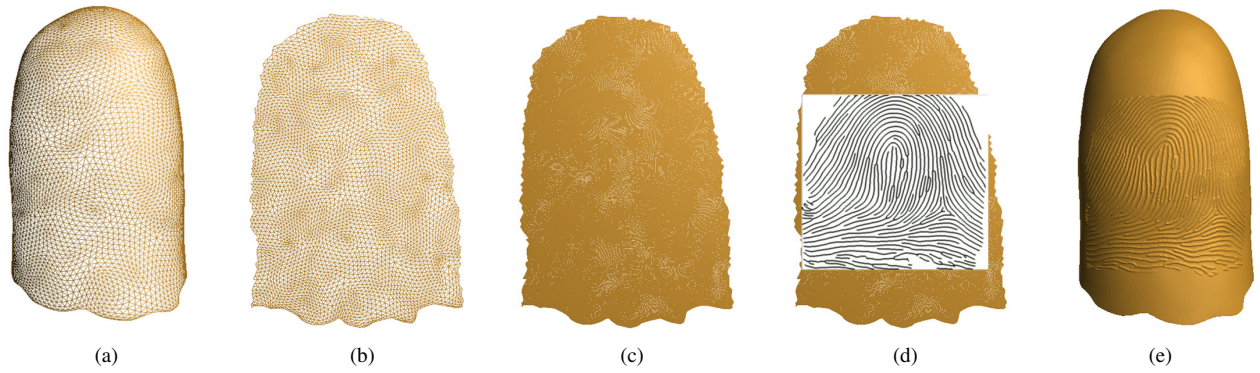
Fig. 6: Mapping and engraving 2D calibration pattern onto the front portion of the outer 3D finger surface S_{OF}. (a) 3D frontal outer finger surface S_{OF}, (b) frontal surface S_{OF} in (a) is projected into 2D, (c) the 2D projected frontal surface S_{OFP} is subdivided, (d) correspondences are determined between the 2D projected frontal finger surface S_{OFP} and 2D calibration pattern I, (e) 3D frontal outer finger surface S_{OF} in (a) is displaced along the surface normals to engrave the pattern.

S_{OF} of the 3D surface to 2D by preserving the geodesic distances between neighborhoood vertices on S_{OF}[6].

Let the 2D projected frontal surface in the (u, v) coordinate space be denoted by S_{OFP} with the set of vertices V_{OFP} and the set of triangles T_{OFP}. Rotation and flip during the 3D to 2D projection of S_{OF} are corrected using corresponding control points between S_{OF} and S_{OFP}. Reference coordinates $[r_u, r_v]$ are extracted from the 2D calibration pattern I for translation correction during the 3D to 2D projection of S_{OF}:

- If the pattern I being projected is a synthetic fingerprint image, then reference coordinates $[r_u, r_v]$ are extracted from the fingerprint image using the method in [28].
- If any other calibration pattern is being projected (e.g. sine gratings, horizontal/vertical bar patterns etc.), then the location of the center pixel in the 2D calibration pattern I is used as the reference point i.e. $[r_u, r_v] = [w/2, h/2]$, where w and h are the width and height of I.

The next step is to determine the one-to-one mapping between the pixel locations (u, v) on I and the vertices V_{OF} on S_{OFP}. For accurately determining the one-to-one correspondence, the density of S_{OF} as well as its 2D projection S_{OFP} is further increased using midpoint surface subdivision. Vertices are sampled on the midpoints of the edges in T_{OF}, and the sampled vertices on the adjacent edges are joined to create new triangles. The resolution of I being projected is factored into the computations while determining the correspondence between pixel locations on I and vertices V_{OF} on S_{OFP}. For example, if the calibration pattern being projected has a resolution of 500 ppi, the scale of projection is 19.685 pixels/mm. Therefore, the coordinates of I are scaled by this factor before determining the correspondence.

Ideally, the density of S_{OF} should be increased according to the dimensions of the calibration pattern I being projected. For example, if a calibration pattern of width w and height h with $w \times h$ pixels is being projected, then exactly $w \times h$ vertices are required in the projection region for building the exact correspondence between the pixel locations on I and the vertices on S_{OF}. However, it would result in a very large number of vertices and triangles on the surface and considerably increase the computational complexity of any further operations on the surface. Therefore, the density of S_{OF} is only increased to the extent that it retains the essential topology of the pattern being projected[7]. Let the set of vertices and triangles on the 2D projected frontal surface obtained after this step be denoted by V_{OFPS} and T_{OFPS}, and the corresponding vertices and triangles on the outer 3D frontal surface be V_{OFS} and T_{OFS}, respectively. The one-to-one correspondence between the pixel locations on the calibration pattern I and the set of vertices V_{OFP} is then established.

D. Engraving 2D calibration pattern on 3D surface

In the penultimate step, surface normals are computed at each vertex in the set V_{OFS}. The vertices are then displaced along their surface normals to engrave the fingerprint ridges and valleys on S_{OF} (see Fig. 6 (e)). Let the normal at a vertex v in the set V_{OFS} be denoted by (n_x, n_y, n_z), where n_x, n_y and n_z represent the normal components along the x, y and z directions, respectively. The displaced coordinates of the vertex (v_x', v_y', v_z') along the normal are then computed using the principle of vertex displacement mapping [29] as follows:

$$\begin{bmatrix} v_x' \\ v_y' \\ v_z' \end{bmatrix} = \begin{bmatrix} v_x \\ v_y \\ v_z \end{bmatrix} + \begin{bmatrix} n_x \\ n_y \\ n_z \end{bmatrix} \times (1 - I'(u, v)) \times R_d \qquad (5)$$

---

[6]Discrete conformal mapping was used for projecting a 2D pattern to 3D finger surface in our preliminary work [1]. It was, however, observed that discrete conformal mapping did not preserve the distances on the calibration pattern near the periphery of the 3D surface since it is an angle preserving mapping.

[7]For the finger surface used in our experiments, the density is increased so that there are approximately 250,000 vertices and 500,000 triangles on the front portion of the 3D surface.
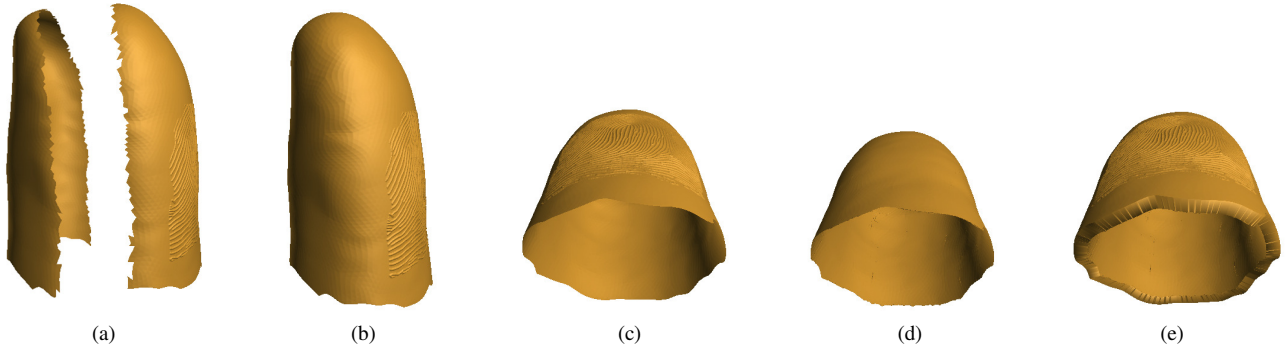
Fig. 7: Postprocessing 3D finger surface. (a) Separated front and rear portions of outer 3D surface, (b) front and rear portions shown in (a) are combined to create the outer 3D finger surface, (c) outer 3D finger surface (bottom view), (d) the retained original 3D finger surface (bottom view), (e) electronic 3D target created by stitching the outer and original surface in (c) and (d).

TABLE II: Comparison of mechanical properties of the two 3D printer materials used for 3D target fabrication with the human finger skin.

Property	Human Skin [30] [31]	TangoBlackPlus FLX980 [32]	FLX 9840 -DM [33]
Shore A hardness	20-41	26-28	35-40
Tensile Strength (MPa)	5-30	0.8-1.5	1.3-1.8
Elongation at Break (%)	35-115	170-220	110-130

Here, $I'(u,v)$ is the scale normalized grayscale value in the range $[0, 1]$ of the mapped grayscale value at (u, v) from the 2D calibration pattern on the vertex corresponding to v in the set V_{OFPS}, and R_d is the maximum vertical ridge displacement which is set to 0.22 mm in our experiments[8].

E. Postprocessing 3D finger surface

The engraved S_{OF} and S_{OR} are combined together to recreate the outer finger surface S'_O. The outer finger surface S'_O is then stitched together with the retained original finger surface S_O to create a continuous watertight 3D shell S_W ready for 3D printing. For doing this, the boundary of the two meshes S'_O and the S_O is first computed. Triangles are then synthetically generated to connect the two boundaries to create a continuous shell (see Fig. 7). This continuous watertight shell is basically the 3D target A in electronic form.

F. 3D printing

We use a state-of-the-art 3D printer (Stratasys Objet350 Connex) that has X and Y resolution of 600 dpi and Z resolution of 1600 dpi for fabricating the 3D targets with rubber-like printing materials. This printer is based on PolyJet printing technology which slices a 3D model into horizontal layers, and then prints the model layer by layer. The 3D targets are printed in high speed mode wherein they are sliced into 30

micrometer (μm) layers during the printing process. Note that the printer does not support printing the target with rubber-like materials in the high resolution mode which allows for even finer 16 micrometer layer slicing. However, we found that 30 μm slicing suffices with ridge displacement R_d of 0.22 mm. In the high speed mode, the time taken to fabricate one 3D target using the printer is approximately 90 minutes. The estimated cost to print a 3D target reported by the printer software is 10-12 dollars.

Two different rubber-like materials, TangoBlackPlus FLX980 [32], and FLX 9840-DM [33] (a digital material synthesized in the printer by combining a rubber-like material and a rigid material) are used for printing the 3D targets. These materials are specifically selected because they are similar in hardness and elasticity to the human finger skin (see Table II)[9]. Note that we are limited in the choice of the printing material per the printer specifications.

Even though the choice of fabrication materials is limited, our approach is better than a manual process of creating a 2.5D or 3D mould of a finger and then casting the targets. This is because the 3D printing process (i) is automated, (ii) can accurately replicate targets, and (iii) is efficient because it can print several targets in parallel.

G. Chemical Cleaning

While printing the 3D targets, the printer uses a support material to prevent the models being fabricated from breaking. As a result, once the targets are printed they need to be cleaned to remove the support material. Manual cleaning removes the bulk of support material, however, still leaves some residue. Therefore, the manually cleaned targets are dipped in a 2M NaOH solution for approx. 3 hours to dissolve the support material residue. Subsequently, the targets are cleaned with water to obtain evaluation-ready 3D targets.

---

[8]The average ridge height on an adult human fingerprint is about 0.06 mm; however we set R_d to 0.22 mm empirically due to limitation of the state-of-the-art 3D printer resolution used for fabricating the targets.

[9]The printing materials used are black in color, and their optical characteristics differ from that of human skin. Therefore, it may not be possible to image the fabricated targets using some optical readers (e.g. dark field readers). To overcome this limitation, we are currently exploring the possibility of using alternative fabrication methods.
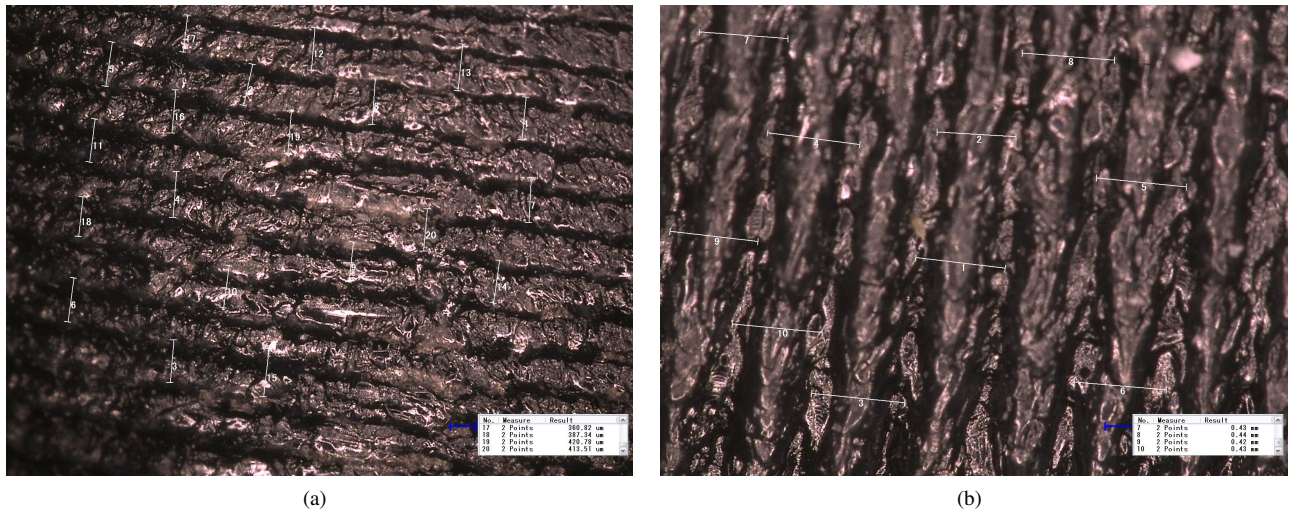
Fig. 8: Estimating 3D printing fabrication error by measuring point-to-point distances between horizontal gratings on a 3D target at (a) 50X and (b) 100X magnification using the Keyence Digital Microscope VHX-600.

TABLE III: Observed average grating spacing on three different targets when viewed under the Keyence VHX-600 Digital Microscope at two different magnifications (50X and 100X). Expected average spacing for each target is 0.478 mm.

Target	50X magnification	100X magnification
Horizontal	0.426 mm	0.427 mm
Vertical	0.420 mm	0.412 mm
Circular	0.415 mm	0.419 mm

III. FIDELITY OF 3D TARGET GENERATION

In order to determine the fidelity of 3D target generation, we measure the error introduced during (i) projection of 2D calibration pattern to 3D surface to create electronic (virtual) target, and (ii) fabrication of physical 3D target from the electronic 3D target using 3D printing. We also conduct experiments to determine the fidelity of 2D pattern features during 3D target creation.

A. 2D to 3D Projection Error

Geodesic distances between all pairs of vertices on the frontal 3D finger surface S_{OF}, and Euclidean distances between the corresponding 2D mapping of vertex pairs after the frontal surface is unwrapped to 2D using the ISOMAP algorithm are computed. Ratio of geodesic distances to euclidean distances is computed to determine the extent to which distances are preserved during 2D to 3D projection. For the finger surface used in our experiments, the geodesic to euclidean distance ratio is estimated as 0.942. This indicates that there is a 5.8% reduction in pairwise (point-to-point) distances due to 2D to 3D mapping algorithm. We account for this error in fingerprint reader evaluation experiments.

B. 3D printing Fabrication Error

Three different 3D targets are created by projecting synthetically generated 2D test patterns: (i) horizontal, (ii) vertical, and (iii) circular gratings, with a fixed center-to-center spacing of 10 pixels. Spacing of 10 pixels in test pattern gratings should correspond to spacing of 0.508 mm in gratings etched on the fabricated physical targets (at the projection scale of 500 ppi). However, the expected average grating spacing on the physical targets is 0.478 (0.508 × 0.942) mm due to the 2D to 3D projection error (5.8%). To measure the observed average grating spacing on the fabricated targets, the three targets are viewed under an optical microscope (Keyence VHX 600 Digital Microscope [17]). Five different images of each of the three targets are captured at two different magnifications of 50X and 100X using the microscope. A total of 20 and 10 point pairs are manually marked on consecutive gratings in images captured at the magnifications of 50X and 100X, respectively. Point-to-point distances are measured between the marked point pairs using the software provided with the microscope (see, for example, Fig. 8). The observed average grating spacing for the three targets at the two magnifications is estimated as the average of the point-to-point distance measurements taken between the manually marked point pairs (see Table III). These measurements indicate that the gratings etched on the physical targets by the 3D printer are much closer to each other than expected or, in other words, grating spacing is reduced upon during 3D fabrication. Based on the difference between the observed and the expected average grating spacing for the three targets, the average reduction in grating spacing due to fabrication is estimated to be 11.42%. Although this error is quite significant, it is expected since we 3D print very fine (0.5 mm) gratings, and the 3D printer is not very accurate in printing objects at such a fine scale. This error is compensated for in fingerprint reader evaluation experiments.

TABLE IV: Similarity scores between the snapshots (2D) of the electronic 3D targets in Meshlab and the 2D fingerprint images from NIST SD4 used for target generation. Verifinger 6.3 SDK was used for generating similarity scores. The threshold on scores @FAR = 0.01% is 33.

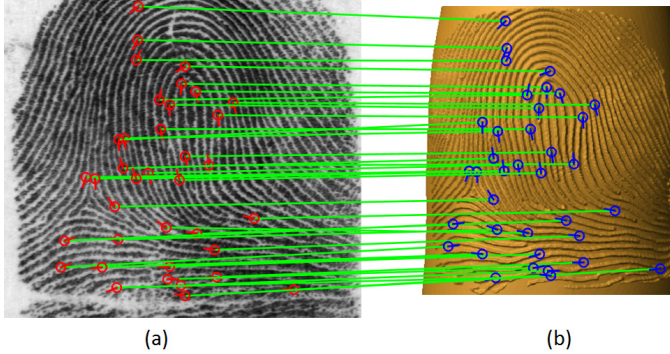| Fingerprint	S0005	S0010	S0017	S0083	S0096
score	171	378	212	116	106

(a)   (b)

Fig. 9: Minutiae correspondence between (a) rolled fingerprint image (S0083 from the NIST SD4), and (b) snapshot of the electronic 3D target generated using (a). Similarity score of 116 is obtained between (a) and (b) which is above the threshold of 33 at 0.01% FAR.

C. Fidelity of 2D pattern features during 3D target creation

To assess if the features in the 2D calibration pattern are adequately preserved during the 3D target generation process, we determine if the

- features present in the 2D calibration pattern, I, are preserved during projection to 3D surface to create the electronic (virtual) 3D target,
- features engraved on the electronic 3D finger surface are preserved after fabrication of the physical 3D target,
- features present in the 2D pattern, I, are preserved on the physical 3D target, and
- intra-class variability between the captured impressions of the 3D target using fingerprint readers is minimal.

Five different rolled fingerprint impressions from the NIST Special Database 4 (NIST SD4) [34] are used as calibration patterns and projected onto a 3D finger surface to generate electronic 3D targets. The physical 3D targets are fabricated with each of the two fabrication materials using a state-of-the-art 3D printer (see Section II-F). Three optical fingerprint readers, abbreviated as OR1, OR2, and OR3 are used for imaging the physical 3D targets[10]. OR1 is a *PIV* certified 500 ppi optical reader, whereas OR2 and OR3 are 1000 ppi optical readers complying with the IAFIS *Appendix F* image quality specifications. A commercial fingerprint SDK [24] is used for conducting all matching experiments. The captured images using the three readers are upsampled by a factor of

---

[10]Capacitive fingerprint readers could not be used in our evaluation because state-of-the-art 3D printers currently do not allow printing objects using conductive materials. We are currently exploring the possibility of using alternative fabrication methods to introduce conductivity.

TABLE V: Similarity scores between the snapshots (2D) of the electronic 3D targets and the images captured by the three optical readers of the physical 3D targets fabricated with two different materials (TangoBlackPlus FLX980 and FLX 9840-DM). Verifinger 6.3 SDK was used for generating similarity scores. The threshold on scores @FAR = 0.01% is 33.

TangoBlackPlus FLX980			
Fingerprint	**OR1 (500 ppi)**	**OR2 (1000 ppi)**	**OR3 (1000 ppi)**
S0005	165	197	392
S0010	192	350	359
S0017	143	180	207
S0083	372	407	348
S0096	165	204	336

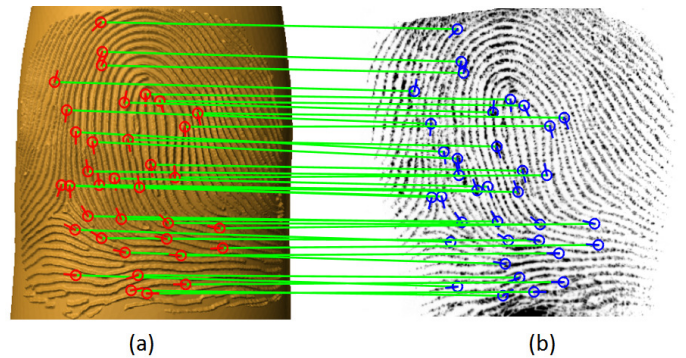| FLX 9840-DM			
Fingerprint	**OR1 (500 ppi)**	**OR2 (1000 ppi)**	**OR3 (1000 ppi)**
S0005	201	342	324
S0010	194	390	342
S0017	143	228	302
S0083	326	473	441
S0096	120	210	179

(a)   (b)

Fig. 10: Minutiae correspondence between (a) snapshot of the electronic 3D target (of fingerprint S0083 in NIST SD4), and (b) the image captured by optical reader 2 (1000 ppi) of the physical 3D target fabricated with FLX 9840-DM. Similarity score of 473 is obtained between (a) and (b) which is above the threshold of 33 at 0.01% FAR.

1.1 to account for ridge spacing reduction due to 2D to 3D projection and 3D printing before conducting the matching experiments.

Fidelity of 2D pattern features after projection to 3D surface: Each electronic 3D target is previewed in the 3D mesh processing software Meshlab [35], and its frontal snapshot[11] is taken. The captured snapshot of the electronic 3D target is rescaled manually to the same scale as the original 2D fingerprint images used during the synthesis of the target. The rescaled snapshot images of the electronic 3D target is matched to the original 2D fingerprint image using the fingerprint SDK.

Fig. 9 shows a sample fingerprint image (calibration pattern) from the NIST SD4 and the snapshot of its electronic 3D target. The minutiae extracted and matched using the fingerprint SDK are marked on the two images. Table IV

---

[11]The term *snapshot* refers to a 2D rendered image of the electronic 3D target.

TABLE VI: Similarity scores between the images captured by the three optical readers of the 3D targets fabricated with two different materials (TangoBlackPlus FLX980 and FLX 9840-DM) and the fingerprints from NIST SD4 used in their generation. Verifinger 6.3 SDK was used for generating similarity scores. The threshold on scores @FAR = 0.01% is 33.

TangoBlackPlus FLX980

Fingerprint	OR1 (500 ppi)	OR2 (1000 ppi)	OR3 (1000 ppi)
S0005	93	161	171
S0010	129	150	183
S0017	93	167	167
S0083	174	344	167
S0096	131	240	197

FLX 9840-DM

Fingerprint	OR1 (500 ppi)	OR2 (1000 ppi)	OR3 (1000 ppi)
S0005	114	410	185
S0010	113	209	173
S0017	122	182	158
S0083	140	374	305
S0096	96	177	177

TABLE VII: Range of similarity scores for pairwise comparisons between five different images captured by the three optical readers of the same 3D target fabricated with two different materials (TangoBlackPlus FLX980 and FLX 9840-DM). Verifinger 6.3 SDK was used for generating similarity scores. The threshold on scores @FAR = 0.01% is 33.

TangoBlackPlus FLX980

Fingerprint	OR1 (500 ppi)	OR2 (1000 ppi)	OR3 (1000 ppi)
S0005	431-1017	675-1146	929-1286
S0010	638-1049	1053-1455	1169-1620
S0017	464-1155	1230-1592	843-1292
S0083	890-1440	1016-1620	744-1325
S0096	726-1286	842-1443	774-1334

FLX 9840-DM

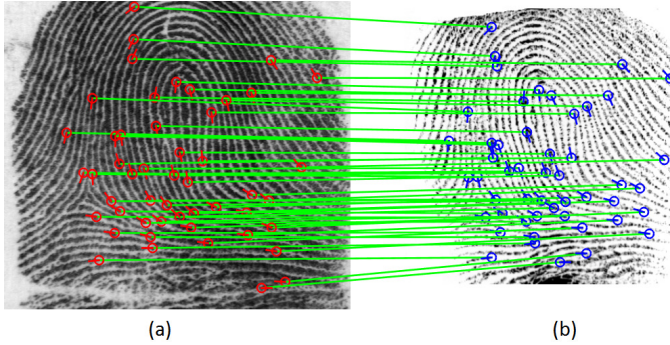| Fingerprint	OR1 (500 ppi)	OR2 (1000 ppi)	OR3 (1000 ppi)
S0005	597-1295	1103-1689	921-1620
S0010	647-1239	1256-1643	1299-1605
S0017	534-1298	1203-1479	1170-1481
S0083	614-1262	1326-1697	1215-1656
S0096	807-1344	1154-1401	1238-1607

(a) (b)

Fig. 11: Minutiae correspondence between (a) rolled fingerprint image (S0083 from the NIST SD4), and (b) the image captured by optical reader 2 (1000 ppi) of the 3D target generated using (a) and fabricated with FLX 9840-DM. Similarity score of 374 is obtained between (a) and (b) which is above the threshold of 33 at 0.01% FAR.
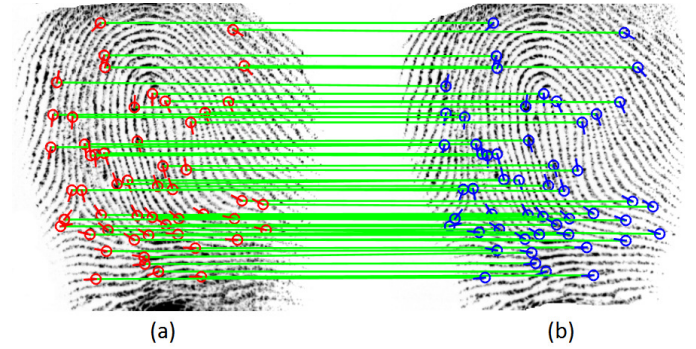

(a) (b)

Fig. 12: Minutiae correspondence between two images (a) and (b) captured by optical reader 2 (1000 ppi) of the 3D target generated from fingerprint S0083 in NIST SD4 and fabricated with FLX 9840-DM. Similarity score of 1494 is obtained between (a) and (b) which is above the threshold of 33 at 0.01% FAR.

shows the corresponding similarity scores. All similarity scores are significantly above the verification score threshold of 33 (@FAR = 0.01%) for NIST SD4. This demonstrates that the features present in the 2D fingerprint images are preserved during the synthesis of the electronic 3D targets.

Fidelity of the engraved features on the 3D surface after 3D printing: The snapshot of an electronic 3D target is matched to captured image of the corresponding physical 3D target using the three optical readers for each of the ten 3D targets. Fig. 10 shows minutiae correspondences obtained using the fingerprint SDK between the snapshot of one electronic target and its captured image using optical reader OR2. Table V shows the similarity scores for this experiment. Notice that the similarity scores are significantly above the verification threshold score of 33 (@FAR = 0.01%) for all ten targets. This demonstrates the fidelity of features engraved on the 3D surface after 3D printing.

End-to-end fidelity of 2D calibration pattern features after 3D printing: Table VI shows the similarity scores obtained when comparing the images of all ten 3D targets captured using the three readers to the corresponding original 2D fingerprint images. Fig. 11 shows minutiae correspondence between the fingerprint image and images of the generated 3D target using the fingerprint SDK. The key observations and inferences based on this experiment are:

- Images of the 3D targets captured using all three optical readers can be successfully matched to the original fingerprint images used for generating the targets; all the similarity scores in Table VI are significantly above the verification threshold score of 33 (@FAR = 0.01%).
- Because the images of the 3D targets can be successfully matched to the original fingerprint images (@FAR = 0.01%), it can be inferred that the salient features present in the 2D pattern are preserved during the fabrication of the physical 3D target.

Intra-class variability between 3D target impressions:
Five different impressions of each of the ten 3D targets are captured using all three optical fingerprint readers. Pairwise comparisons between the five impressions obtained from a fingerprint reader are performed using the fingerprint SDK. Fig. 12 shows the minutiae correspondence between two different impressions of a 3D target captured using optical reader OR2. Table VII shows the range of similarity scores all of which are significantly higher than the threshold at 0.01% FAR. This indicates that the intra-class variability between different images of the 3D target is small.

IV. BEHAVIORAL EVALUATION OF FINGERPRINT READERS USING 3D TARGETS

We conduct two different experiments to show the utility of the fabricated 3D targets for behavioral evaluation of fingerprint readers, (i) using 3D targets created from synthetically generated test patterns to evaluate directional imaging capability (Experiment I), and (ii) using 3D targets created by projecting fingerprint patterns to evaluate the capability to capture fingerprint patterns (Experiment II). The synthetic test patterns provide a reference from which pattern replication errors are measured, analogous to the use of image quality test patterns for evaluating other imaging technologies. Additionally, the coordinate locations of all features in the generated synthetic test patterns are known exactly and this facilitates reproducible computation of replication errors and supports the development of measurement uncertainties.

A. Experiment I

Ten different impressions of each of the three targets created using horizontal, vertical and circular sine gratings of 10 pixel spacing are captured using all three optical readers. Center-to-center spacing is then measured in each of the captured impressions using the method in [36]. Directional imaging capability of fingerprint readers is subsequently assessed based on how well the grating spacing on the three targets is recovered by the readers. Figs. 13, 14 and 15 show the three directional test patterns, the electronic targets generated using the three patterns, and some sample images of the three targets captured using the three optical readers. The average and the standard deviation of the observed center-to-center grating spacing in the captured impressions of the three targets is reported in Table VIII. Note that the expected grating spacing on these targets is 8.278 (10×0.827) pixels after taking into account the reduction in spacing due to projection (5.8%) and fabrication error (11.42%). Following are some observations based on this experiment:

- The computed spacing in images of all three targets is observed to be greater than the expected spacing. Since we account for the 2D to 3D projection and 3D fabrication errors in our spacing measurements, this difference should be due to the flattening of 3D target gratings when the target is pressed against the reader platen.
- The deviation from the expected spacing is found to be greater for the circular target than the horizontal and

TABLE VIII: Mean (μ) and std. deviation (σ) of center-to-center spacing in the images of the three directional test targets captured using the three optical readers (OR). (Expected grating spacing = 8.278 pixels.)

Test pattern	OR1 (500 ppi)	OR2 (1000 ppi)	OR3 (1000 ppi)
Horizontal	$\mu = 8.307, \sigma = 0.101$	$\mu = 8.445, \sigma = 0.085$	$\mu = 8.420, \sigma = 0.030$
Vertical	$\mu = 8.869, \sigma = 0.076$	$\mu = 8.561, \sigma = 0.076$	$\mu = 8.592, \sigma = 0.098$
Circular	$\mu = 8.921, \sigma = 0.044$	$\mu = 8.823, \sigma = 0.048$	$\mu = 8.721, \sigma = 0.053$

vertical targets. This can be explained by the fact that the characteristic flattening induced when the target is pressed against the reader platen is radial around the central point of contact. In other words, target regions closer to the central point of contact with the reader platen flatten out more compared to surrounding regions. The relative effect of such a flattening is not as profound on both horizontal and vertical gratings compared to circular gratings because the circular gratings align symmetrically with the radial flattening.

- The horizontal target spacing captured by all three readers is observed to be closest to the expected spacing compared to vertical and circular targets. This may be due to the way pressure is applied on the reader platen with respect to the relative orientation of the gratings while capturing the target images. Controlled experimentation, where both the magnitude and direction of pressure applied on the reader platen is fixed before capturing the target impressions, is required to understand the underlying cause, which will be undertaken in future studies.

Although the primary use for the 3D targets generated here is to measure the image capture fidelity of fingerprint readers, targets created with test patterns and fabrication materials different from those used in this study, may have other potential metrology applications. For example, the 3D targets may provide a means for calibrating the dimensional measurements

TABLE IX: Mean (μ) and std. deviation (σ) of center-to-center ridge spacing in the fingerprint target images captured using the three optical readers (OR). The expected average ridge spacing (in pixels) in the target images is indicated in brackets.

TangoBlackPlus FLX980			
Test pattern	OR1 (500 ppi)	OR2 (1000 ppi)	OR3 (1000 ppi)
S0005 (7.818)	$\mu = 8.493, \sigma = 0.096$	$\mu = 8.250, \sigma = 0.048$	$\mu = 8.099, \sigma = 0.054$
S0010 (8.433)	$\mu = 9.215, \sigma = 0.156$	$\mu = 9.172, \sigma = 0.024$	$\mu = 9.128, \sigma = 0.053$
S0017 (8.932)	$\mu = 9.893, \sigma = 0.118$	$\mu = 9.525, \sigma = 0.038$	$\mu = 9.523, \sigma = 0.136$
S0083 (8.621)	$\mu = 9.100, \sigma = 0.191$	$\mu = 9.111, \sigma = 0.057$	$\mu = 9.110, \sigma = 0.190$
S0096 (8.473)	$\mu = 8.817, \sigma = 0.056$	$\mu = 8.839, \sigma = 0.075$	$\mu = 8.670, \sigma = 0.102$

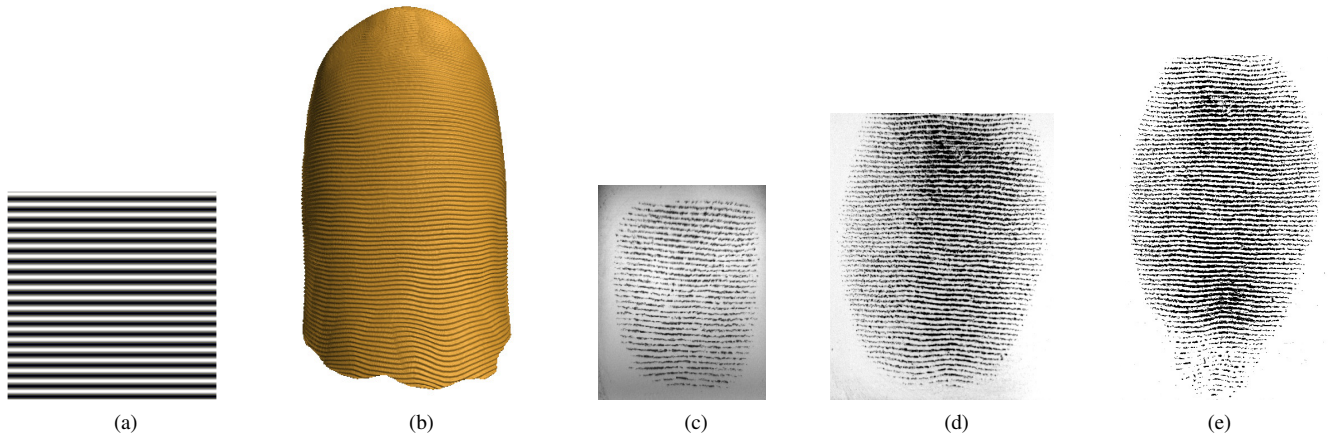| FLX 9840-DM			
Test pattern	OR1 (500 ppi)	OR2 (1000 ppi)	OR3 (1000 ppi)
S0005 (7.818)	$\mu = 8.440, \sigma = 0.129$	$\mu = 8.288, \sigma = 0.011$	$\mu = 8.135, \sigma = 0.079$
S0010 (8.433)	$\mu = 9.559, \sigma = 0.065$	$\mu = 9.168, \sigma = 0.052$	$\mu = 9.077, \sigma = 0.048$
S0017 (8.932)	$\mu = 9.988, \sigma = 0.073$	$\mu = 9.539, \sigma = 0.032$	$\mu = 9.565, \sigma = 0.055$
S0083 (8.621)	$\mu = 9.302, \sigma = 0.061$	$\mu = 9.131, \sigma = 0.037$	$\mu = 9.080, \sigma = 0.042$
S0096 (8.473)	$\mu = 8.752, \sigma = 0.102$	$\mu = 8.772, \sigma = 0.063$	$\mu = 8.654, \sigma = 0.063$

Fig. 13: Evaluating fingerprint readers with a 3D target generated using a horizontal sine grating. (a) Horizontal sine grating (10 pixel separation between the gratings); (b) electronic 3D target generated using (a); (c), (d) and (e) are sample images of the fabricated target captured using optical readers 1, 2 and 3, respectively. There is a slight distortion apparent in (b) that is due to the 2D to 3D projection error.
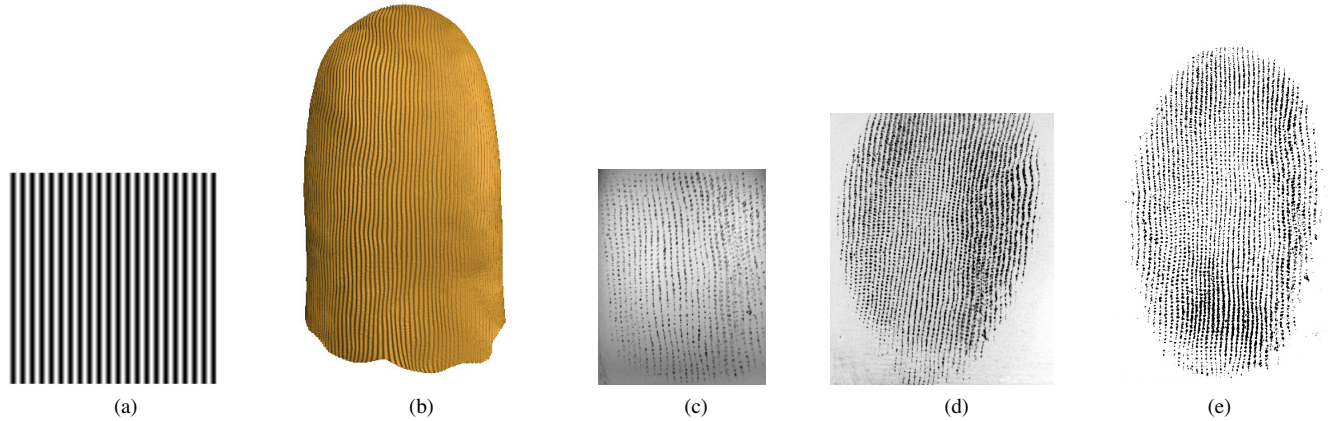

Fig. 14: Evaluating fingerprint readers with a 3D target generated using a vertical sine grating. (a) Vertical sine grating (10 pixel separation between the gratings); (b) electronic 3D target generated using (a); (c), (d) and (e) are sample images of the fabricated target captured using optical readers 1, 2 and 3, respectively. There is a slight distortion apparent in (b) that is due to the 2D to 3D projection error.

of optical-microscopy-based surface profilometers described for measuring fingerprint patterns [37] [38] because these targets have patterns with known feature coordinate locations and known geometric relationship between these features.

B. Experiment II

The ten 3D targets generated by projecting five different fingerprint images from NIST SD4 and fabricated using each of the two printing materials are used to evaluate the imaging capability of the three fingerprint readers to capture fingerprint patterns. Center-to-center ridge spacing is computed on the original 2D fingerprint pattern that is used to create each target using the method in [36]. Analogous to Experiment I, the average and variance of center-to-center ridge spacing values is computed for five different 2D impressions of each target captured using the three optical readers. Note that the same method [36] is used to compute ridge spacing on the

captured 2D plain impressions of the targets. Table IX shows the computed ridge spacing measurements. Following are the main observations based on this experiment:

- The 1000 ppi readers OR2 and OR3 are, on average, better than the 500 ppi reader in preserving fingerprint ridge spacing. This may be due to lesser ridge flattening being induced by the reader platens for these two readers compared to OR1. Amongst the two 1000 ppi readers, OR3 seems to perform marginally better, on an average, than OR2 in preserving fingerprint ridge spacing.

- The 500 ppi reader OR1 has a small platen and is only able to partially image the fingerprint targets. Therefore, overall fewer spacing measurements are used for average spacing computations and the variation in spacing is relatively higher for the reader OR1 than the readers OR2 and OR3.
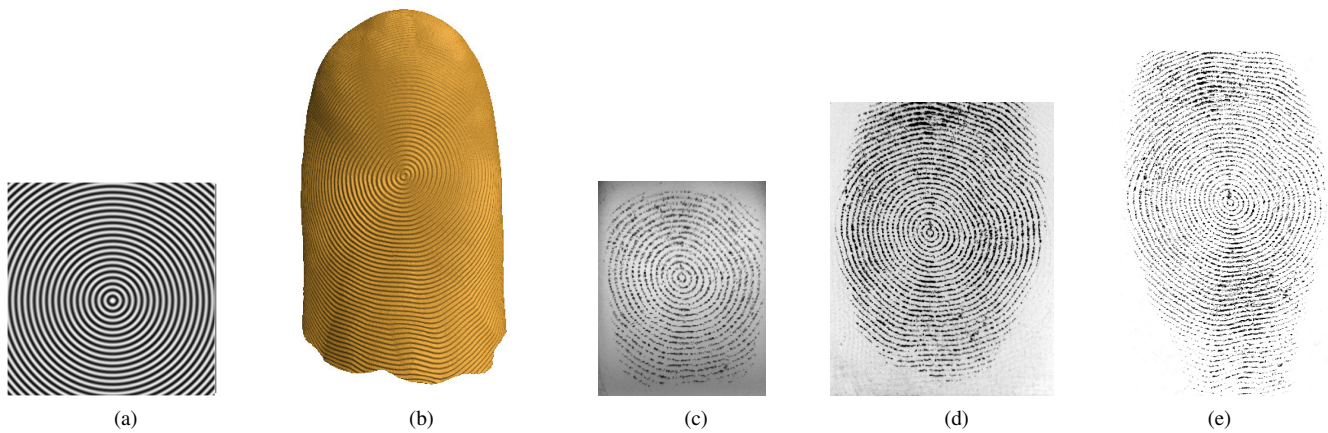
Fig. 15: Evaluating fingerprint readers with a 3D target generated using a circular sine grating. (a) Circular sine grating (10 pixel separation between the gratings); (b) electronic 3D target generated using (a); (c), (d) and (e) are sample images of the fabricated target captured using optical readers 1, 2 and 3, respectively. There is a slight distortion apparent in (b) that is due to the 2D to 3D projection error.

- There is no significant impact of the fabrication material on the ridge spacing measurements in fingerprint images captured using the three readers.

All three optical readers used for conducting experiments are *PIV/Appendix F* certified. Note, however, that the errors obtained in our evaluation experiments are comparatively greater than permitted geometric errors for the *PIV* and *Appendix F* standards. This is because of the flattening of the patterns on the 3D targets when they are pressed against the reader platens. The current certification standards do not explicitly account for this error. However, it is important to consider this error in the operational scenario where user-dependent parameters, such as finger placement and pressure applied on the reader platen, directly impact the fingerprint image acquired by a fingerprint reader.

V. CONCLUSIONS AND ONGOING WORK

Structural evaluation of fingerprint readers is typically done using 2D or 3D targets designed for calibrating imaging devices. While these targets are used for structural evaluation of fingerprint readers, they cannot be used for behavioral evaluation of fingerprint readers in operational scenarios. In this research, we have designed and fabricated wearable 3D fingerprint targets that can be placed on the fingerprint reader platen, and imaged analogous to operational setting where a user's finger will interact with the reader. The 3D targets are created by projecting 2D calibration patterns of known characteristics (e.g. sine gratings of known spacing) onto a generic 3D finger surface to generate electronic 3D targets. The electronic targets are then fabricated using a state-of-the-art 3D printer with material similar in hardness and elasticity to the human finger skin. Our experimental results show that (i) features present in the 2D calibration pattern are preserved during the creation of electronic 3D target, (ii) features engraved on the electronic 3D target are preserved during physical 3D target fabrication, and (iii) intra-class variability between multiple images of the same physical 3D target is sufficiently small for

matching at 0.01% FAR. We also show that the generated 3D targets can be used for behavioral evaluation of three different (500/1000 ppi) PIV/Appendix F certified optical fingerprint readers in the operational settings.

We are making attempts to find materials with similar conductive properties to the human finger skin to generate 3D targets for evaluating capacitive fingerprint readers. In future, we plan to explore generating 3D targets by creating a 3D mould from the 2D calibration pattern and then casting the targets. We also plan to simulate the effects of dry and worn out fingers using 3D targets with different depths of engravings to further study the imaging capabilities of different readers.

REFERENCES

[1] S. S. Arora *et al.*, "3D Fingerprint Phantoms," in *22nd International Conference on Pattern Recognition (ICPR)*, 2014, pp. 684–689.

[2] R. Black, *Managing the Testing Process*. John Wiley & Sons, 2002.

[3] V. V. Tuchin *et al.*, "Finger tissue model and blood perfused skin tissue phantom," pp. 78 980Z–78 980Z–11, 2011. [Online]. Available: http://dx.doi.org/10.1117/12.881604

[4] D. A. Boas, C. Pitris, and N. Ramanujam, *Handbook of Biomedical Optics*. Taylor & Francis, 2011.

[5] "FBI Biospecs IAFIS FAQs," https://www.fbibiospecs.org/iafis_faq.html.

[6] N. B. Nill, "Test procedures for verifying image quality requirements for personal identity verification (PIV) single finger capture devices," MITRE, Tech. Rep. MTR 060170, 2006.

[7] ——, "Test procedures for verifying IAFIS image quality requirements for fingerprint scanners and printers v 1.4," MITRE, Tech. Rep. MTR 05B0016R7, 2013.

[8] "FBI IAFIS certified product listing," http://www.fbi.gov/about-us/cjis/fingerprints_biometrics/iafis/iafis_cert.

[9] "Thor Labs Calibration Targets," http://www.thorlabs.com/newgrouppage9.cfm?objectgroup_id=7502.

[10] R. Cappelli, "SFinGe: an approach to synthetic fingerprint generation," in *International Workshop on Biometric Technologies (BT2004)*, 2004, pp. 147–154.

[11] IBG, "Synthetic biometric image generator," *Department of Homeland Security Small Business Innovation Research Final Report*, 2012.

[12] Q. Zhao *et al.*, "Fingerprint image synthesis based on statistical feature models," in *IEEE Fifth International Conference on Biometrics: Theory, Applications and Systems (BTAS)*, 2012, pp. 23–30.

[13] "ONEprint touchless fingerprint reader," http://www.idairco.com/products/.

[14] "FlashScan3D touchless fingerprint sensor," http://www.flashscan3d.com/.

[15] "Morpho Finger on the Fly," http://www.morpho.com/identification/border-control-242/semi-automated-control/finger-on-the-fly-r-946/?lang=en.

[16] "Artec Eva 3D scanner," http://www.artec3d.com/hardware/artec-eva/.

[17] "Keyence Digital Microscope VHX-600," http://www1.keyence.eu/products/microscope/microscope/vhx6002/vhx6002_specifications_1.php.

[18] I. Jolliffe, *Principal Component Analysis*.　Wiley Online Library, 2005.

[19] G. Peyré and L. D. Cohen, "Geodesic remeshing using front propagation," *International Journal of Computer Vision*, vol. 69, no. 1, pp. 145–156, 2006.

[20] R. Kimmel and J. A. Sethian, "Computing geodesic paths on manifolds," *Proceedings of the National Academy of Sciences*, vol. 95, no. 15, pp. 8431–8435, 1998.

[21] P. Alliez *et al.*, "Anisotropic polygonal remeshing," in *ACM Transactions on Graphics (TOG)*, vol. 22, no. 3.　ACM, 2003, pp. 485–493.

[22] N. Amenta *et al.*, "The crust and the β-skeleton: Combinatorial curve reconstruction," *Graphical Models and Image Processing*, vol. 60, no. 2, pp. 125–135, 1998.

[23] C. Loop, "Smooth subdivision surfaces based on triangles," Master's thesis, University of Utah, 1987.

[24] "Neurotechnology Verifinger SDK 6.3," http://www.neurotechnology.com/verifinger.html.

[25] J. B. Tenenbaum *et al.*, "A global geometric framework for nonlinear dimensionality reduction," *Science*, vol. 290, no. 5500, pp. 2319–2323, 2000.

[26] E. Dijkstra, "A note on two problems in connexion with graphs," *Numerische Mathematik*, vol. 1, no. 1, pp. 269–271, 1959. [Online]. Available: http://dx.doi.org/10.1007/BF01386390

[27] J. B. Kruskal and M. Wish, *Multidimensional Scaling*.　Sage, 1978.

[28] S. Yoon *et al.*, "LFIQ: Latent fingerprint image quality," in *IEEE Sixth International Conference on Biometrics: Theory, Applications and Systems (BTAS)*, 2013, pp. 1–8.

[29] "Vertex Displacement Mapping using GLSL," http://www.ozone3d.net/tutorials/vertex_displacement_mapping_p02.php.

[30] C. Edwards and R. Marks, "Evaluation of biomechanical properties of human skin," *Clinics in Dermatology*, vol. 13, no. 4, pp. 375–380, 1995.

[31] V. Falanga and B. Bucalo, "Use of a durometer to assess skin hardness," *Journal of the American Academy of Dermatology*, vol. 29, no. 1, pp. 47–51, 1993.

[32] "Stratasys Polyjet Material Data Sheet," http://www.stratasys.com/~/media/Main/Secure/Material%20Specs%20MS/PolyJet-Material-Specs/PolyJet_Materials_Data_Sheet.pdf.

[33] "Stratasys Digital Materials (DMs) Data Sheet," http://www.stratasys.com/~/media/Main/Secure/Material%20Specs%20MS/PolyJet-Material-Specs/Digital_Materials_Datasheet.pdf.

[34] "NIST Special Database 4," http://www.nist.gov/srd/nistsd4.cfm.

[35] "Meshlab," http://sourceforge.net/projects/meshlab/.

[36] L. Hong *et al.*, "Fingerprint image enhancement: algorithm and performance evaluation," *IEEE Transactions on Pattern Analysis and Machine Intelligence*, vol. 20, no. 8, pp. 777–789, 1998.

[37] G. Balogiannis *et al.*, "A computer vision non-contact 3D system to improve fingerprint acquisition," *International Journal of Computer (IJC)*, vol. 20, no. 1, pp. 174–198, 2016.

[38] S. Huang *et al.*, "3D fingerprint imaging system based on full-field fringe projection profilometry," *Optics and Lasers in Engineering*, vol. 52, pp. 123–130, 2014.

Sunpreet S. Arora received the Bachelor of Technology (Hons.) degree in Computer Science from the Indraprastha Institute of Information Technology, Delhi (IIIT-D) in 2012. He is currently a doctoral student in the Department of Computer Science and Engineering at Michigan State University. His research interests include biometrics, pattern recognition and image processing. He received the best poster award at the IEEE Fifth International Conference on Biometrics: Theory, Applications and Systems (BTAS), 2012. He is a student member of the IEEE.
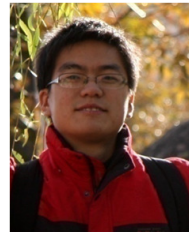
Kai Cao received the Ph.D. degree from Key Laboratory of Complex Systems and Intelligence Science, Institute of Automation, Chinese Academy of Sciences, Beijing, China, in 2010. He is currently a Post Doctoral Fellow in the Department of Computer Science & Engineering, Michigan State University, East Lansing. His research interests include biometric recognition, image processing and machine learning.

Anil K. Jain is a University distinguished professor in the Department of Computer Science and Engineering at Michigan State University. His research interests include pattern recognition and biometric authentication. He served as the editor-in-chief of the IEEE Transactions on Pattern Analysis and Machine Intelligence (1991-1994). He served as a member of the United States Defense Science Board and The National Academies committees on Whither Biometrics and Improvised Explosive Devices. He has received Fulbright, Guggenheim, Alexander von Humboldt, and IAPR King Sun Fu awards. He was elected to the National Academy of Engineering in 2016.

Nicholas G. Paulter Jr. is the Group Leader for the Security Technologies Group at NIST in Gaithersburg, MD. He develops and oversees metrology programs related to concealed weapon and contraband imaging and detection, biometrics for identification, and body armor characterization. He has authored or co-authored over 100 peer-reviewed technical articles and provided numerous presentations at a variety of technical conferences. He is a 2008-2009 Commerce Science and Technology Fellow and a 2010 IEEE Fellow.